J. Min. Metall. Sect. B-Metall. 59 (2) (2023) 287 - 297

Journal of Mining and Metallurgy, Section B: Metallurgy

INFLUENCE OF MICROSTRUCTURE AND CRYSTALLOGRAPHIC TEXTURE ON HYDROGEN DIFFUSION IN IF-STEEL

Ü. Başkaya [a*], R. Uzun [a], K. Davut [b], Y. Kiliç [a], O. Gündüz [a]

[a] Eregli Iron and Steel Works Co., R&D Center, 67300, Kdz. Eregli, Zonguldak, Turkey
[b] Department of Materials Science and Engineering, Izmir Institute of Technology, Urla, Izmir, Turkey

(Received 01 February 2023; Accepted 17 August 2023)

Abstract

The relation between microstructure, crystallographic texture, and hydrogen diffusion was studied on a IF-steel. The steel samples were deep drawn to a strain level of 10%, 20%, 30% and 40% and then the hydrogen diffusion coefficients were determined using the Helios II system. Light optical microscope (LOM), scanning electron microscope (SEM) and electron backscatter diffraction (EBSD) were used for microstructural characterization and crystallographic texture studies. The dependence of microstructural parameters was evaluated by Pearson correlation coefficient (PCC) values. These evaluations showed that local misorientations, crystallographic texture, and dislocation densityare interdependent. The PCC values show that grain size and dislocation density are the independent microstructure related parameters. These parameters were used to build a model to predict the hydrogen diffusion coefficient by multiple linear regression analysis. A sensitivity analysis was also performed with this model to understand to which parameter the hydrogen diffusion is most sensitive. The results of this analysis show that hydrogen diffusion is more sensitive to dislocation density, suggesting that dislocations are more effective trapping sites for hydrogen atoms. On the other hand, grain boundaries are less effective trapping sites since they also provide an additional diffusion mechanism.

Keywords: *Low carbon enameled steel; Deep drawing; Hydrogen permeability; Microstructure; Crystallographic texture; Multiple linear regression analysis; Sensitivity analysis*

1. Introduction

Carbon steels are widely used in industry due to their good formability, weldability, and suitability for enamel coating [1-5]. Despite their widespread usage, those steel grades experience catastrophic failures due to hydrogen. High strength and pipeline steels (especially after welding) are more prone to hydrogen embrittlement and delayed cracking [6-9]. In addition to embrittlement, hydrogen can also cause problems in coated and painted steels, the most common of which is fish scale defect. Fish scale defect is delayering of coatings, which is induced by dissolving of excess hydrogen during firing and painting stages [4]. Since its solubility gradually decreases during subsequent cooling, the hydrogen moves towards the steel coating interface, where it's the high pressure cause the coatings scales to detach [4, 10, 11]. Hydrogen induced problems can occur days or even months after the coating or forming processes. Once the defect appears, it is almost impossible to recover [12-14].

Most studies concentrate on the relation between embrittlementorscaling and hydrogen permeability. Increasing the amount of precipitates, inclusions, and dislocations and decreasing the grain size improves hydrogen permeability. Grain boundaries, precipitates, inclusions, and dislocations can act as hydrogen trapping sites and their fraction should be increased to reduce the likelihood of hydrogen related problems [15-23]. Barsanti et al. [24] analyzed the effect of steel thickness on hydrogen permeability using mathematical and statistical methods and found that the diffusion coefficient decreases with steel thickness, which in turn decreases the probability of fish scale formation. Yi et al. [16] evaluated the effects of the continuous annealing process parameters on the final product properties.

It was determined that the ferrite grain size and precipitate size increased and the number of precipitates decreased as the soaking temperature increased. It was reported that the changes in the microstructure reduced the hydrogen diffusion time and negatively affected the permeability property. However, in the related study, there was insuffici-entinformation onwhich precipitate type exhibited dominant behavior and the varying amounts of precipitate per unit area. Leveaux et al. [15] reported that the diffusion coefficient increases with increasing process temperature due to decreasing number of the

Corresponding author: uebaskaya@gmail.com

https://doi.org/10.2298/JMMB230201025B

trapping sites. Fábián and Szabó [25] showed that dislocation density and <111> // normal direction (ND) fiber texture act as a hydrogen trapping site. In another study by Fábián [26], it was reported that the dislocation density below 25% thickness reduction did not act as a major trapping site. It was showed that the hydrogen permeability property changes as a function of the dislocation character, dislocation density, carbide sizes and carbide position.

Previous studies showed that grain boundaries, dislocations, and precipitates can act as hydrogen trapping sites and affecthydrogen permeability. Moreover, thesteel thickness and crystallographic texture were also reported to influence hydrogen permeability. The effects of different microstructural parameters (grain size, dislocation density, crystallographic texture, type and number of precipitates etc.) on hydrogen permeability behavior had been investigated individually. However, there is no study that considers all microstructural parameters and quantifies their relation with hydrogen permeability. This study aims at closing this gap by evaluating the relation between the microstructural parameters and hydrogen permeability using "multiple linear regression analysis" (MLRA). Moreover, a sensitivity analysis is performed to understand which microstructural feature hydrogen permeability is most sensitive to.

2. Material and Methods

2.1. Material

Titanium (Ti) stabilized ultra-low carbon DC06ED cold rolled and annealed steel grade was used in this study. The thickness of this interstitial free (IF) steel sample is 0.80 mm and its chemical composition is given in Table 1.

Table 1. *Chemical analysis of steel (wt.%)*

Steel grade	C	Mn	P	S	Al	Ti
DC06ED	0.003	0.082	0.017	0.02	0.06	0.075

2.2. Microstructural characterization

Samples were cut in transverse direction (TD) – normal direction (ND) plane, hot mounted, grinded and polished respectively. After the sample preparation process, they were etched with Marshall solution for characterization. The cross section of samples was analyzed by using light optical microscope (Nikon Eclipse MA200) and SEM (JSM-7100F).

The polishing stages of the samples to be used in EBSD (Oxford Nordlys Nano EBSD detector) analysis was different and colloidal silica solution (0.05 μm) was used in the last stage of polishing. For texture characterization, EBSD measurements were performed and all measurements were carried out in the TD plane. Working distance, acceleration voltage, and step size were selected as 17 mm, 20 kV and 0.1 μm respectively for EBSD conditions.

2.3. Forming simulation and hydrogen permeation test

The hydrogen permeability coefficient is generally measured in the plate form of steel. However, to interpret it for industrially relevant conditions, hydrogen permeability tests were performed by simulating the forming process before enamel coating.

The deep drawing test machine (Zwick BUP600) was used to simulate typical industrial forming process before enamel coating. Marciniak Test was carried out according to ISO 12004 until 4 different strain levels, which are 10 %, 20 %, 30 % and 40 %. The machine was connected to a GOM/Aramis optical strain measurement system. Data collection and processing for strain ratio calculations were performed via Aramis software [27]. Strain levels are determined from the center of the formed cup where the maximum strain levels are reached during the test period.

Hydrogen permeability test samples were cut from deep drawn samples. Hydrogen permeation test sample (50x120 mm) was taken from the steel after Marciniak test, as shown in Figure 1. Helios II test device was used for hydrogen permeation tests at room temperature. The equipment is based on a solid-state gas sensor and is able to perform electrochemical permeation of metal samples [6]. Hydrogen diffusion coefficients were also determined with those tests. The hydrogen diffusion coefficient D (cm^2/s) is calculated as shown in the following equation. In this formula, d represents the thickness (cm) of the sample and $t_{63}\%$ represents the time (second). There are four different methods for evaluating the hydrogen diffusion coefficient through the steels. One of them is 63% method, according to ASTM G148 – 97 [29]. t63 (sec) is the time where the flux of hydrogen reaches the 63% of the steady state.

$$D = \left(d^2 / t_{63}\%\right) \cdot 6 \quad (1)$$

3. Results

3.1. Hydrogen permeability properties

The results of the hydrogen permeation test are given in Table 2 and the hydrogen permeability curves of the samples are given in Figure 2. Monitoring

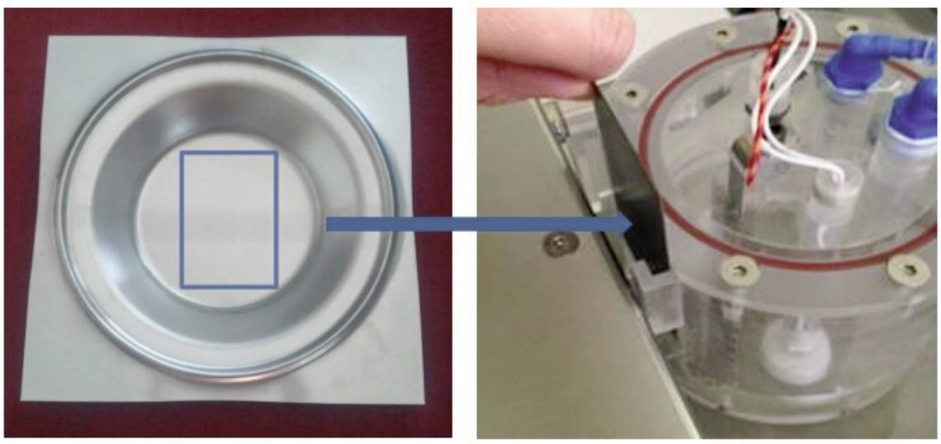

Figure 1. *(a) Deep drawing test sample and (b) position of the sample in the hydrogen permeability test cabinet*

hydrogen flux is particularly relevant for risk migration of elements involved in hydrogen storage and transportation [30]. The tabulated results show that the hydrogen diffusion coefficient decreased and the permeability time increased depending on the increasing of strain value. While the hydrogen diffusion coefficient of non-deformed sample is $0.82x10^{-6}$ cm^2/s, the diffusion coefficient decreases up to $0.34x10^{-6}$ cm^2/s at 40% strain value.

Table 2. *Result of hydrogen permeation test*

Strain (%)	Hydrogen diffusion coefficient	Hydrogen diffusion time
	(cm^2/sec)	(sec)
0	$0.82x10^{-6}$	1591
10	$0.63x10^{-6}$	1555
20	$0.53x10^{-6}$	1640
30	$0.40x10^{-6}$	1897
40	$0.34x10^{-6}$	2137

3.2. Microstructural characterization and crystallographic texture analysis

The undeformed sample is composed of equiaxed ferrite grains, as shown in the LOM micrograph given in Figure 3. The grain orientation spread (GOS) map of the undeformed sample is given in Figure 3, and GOS maps of deformed samples are given in Figure 4. GOS values define grain based local misorientations and to calculate it first the average orientation of a grain is calculated. Then the misorientation between this average orientation and the orientation of each individual measurement point within the grain is calculated. The average of these misorientations gives the grain orientation spread of that grain. The GOS distributions were also determined for all samples and

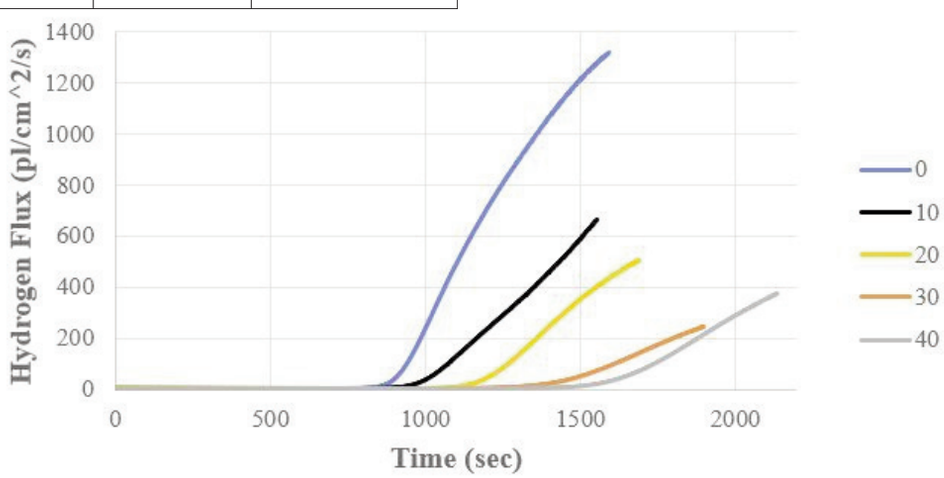

Figure 2. *Hydrogen permeability curves of the samples applied with different deformation amounts (nondeformed, 10%, 20%, 30%, 40%)*

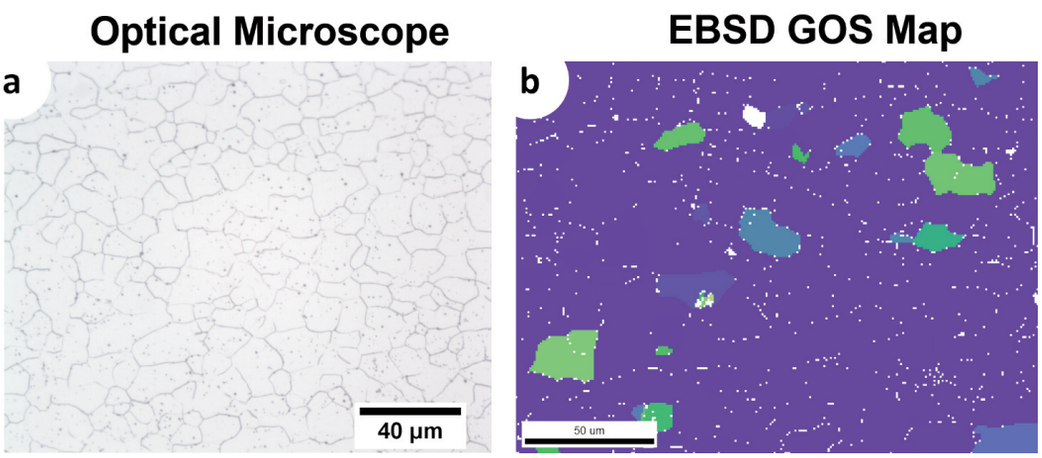

Figure 3. *a) LOM micrograph, b) grain orientation spread (GOS) of undeformed sample*

given in Figure 5a. Almost all of the grains of the undeformed sample have GOS values of 0, or near 0. Since this sample contains fully recrystallized grains GOS values are close to 0. On the other hand, the GOS values increase with increasing strain levels. GOS values show misorientations grain by grain. The local misorientations, also the misorientations within a grain are given by the kernel average misorientation (KAM) value. The KAM distributions of samples were given in Figure 5b. The KAM value is calculated for each point in the EBSD map. The average misorientation of a point with respect to all its neighbors is calculated while misorientations higher than 5° are regarded as grain boundaries in accordance with the ASTM E2627 standard [31] and excluded from KAM calculations. Misorienations higher than 15o are high angle grain boundaries and lower degree misorientations are low angle grain boundaries [32-33]. For the present steel, majority of grain boundaries (>80%) are high angle grain boundaries. Misorientations (KAM and GOS values) increase with defect (i.e. dislocation) densities, which also increases with strain.

Geometrically necessary dislocations (GNDs) accommodate orientation gradients within the grains; therefore, they are required to maintain lattice continuity [34]. Orientation gradients such as KAM values can be calculated from EBSD data since it

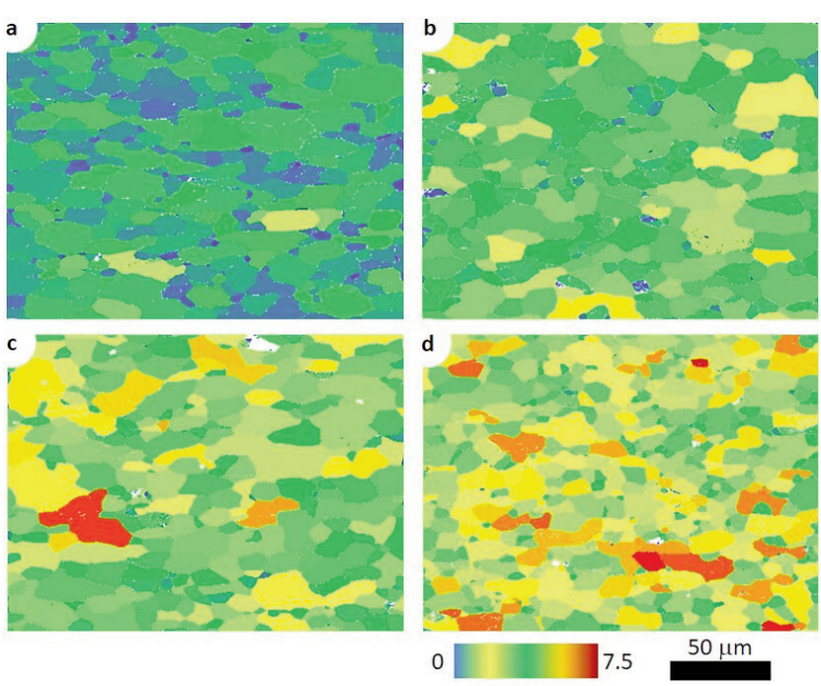

Figure 4. *Grain orientation spread maps of samples deformed to a) 10%, b) 20%, c) 30% and d) 40% strain levels*

contains point by point orientation information at sub-grain size scale. By knowing the orientation of the crystal in relation to the orientation gradient together with slip and slip plane normal directions (i.e. slip system), GND density can be calculated as shown elsewhere [35-37].

GND density distributions of samples are given in Figure 5c. The GND densities increase with increasing strain. Moreover, the grain size distributions are also determined and given in Figure 5d. The average grain size of the samples does not change significantly. On the other hand, the distributions show broadening, particularly the fraction of smaller grains increase. Deformation increases local misorientations and causes formation of sub-structures [38], which are identified as separate grains with lower average misorientations.

Electron Back Scattered Diffraction (EBSD) data can also be used to determine the crystallographic texture. For body-centered-cubic (BCC) materials α- and γ-fibers are the most commonly observed texture fibers, especially for the cold rolled and annealed samples. The texture intensity distributions along α- and γ-fibers are given in Figure 6. Usually, deformation intensifies α-fiber and recrystallization intensifies γ-fiber [39]. For the present samples, both the average and maximum intensity values along α-fiber increase with strain. The (111) <110> texture component is common for α- and γ-fibers, therefore γ-fiber intensity does not change regularly in the samples since there is no additional recrystallization occurs during deformation of the samples and some components of γ-fiber actually increase with deformation. All of the microstructure related data is tabulated in Table 3.

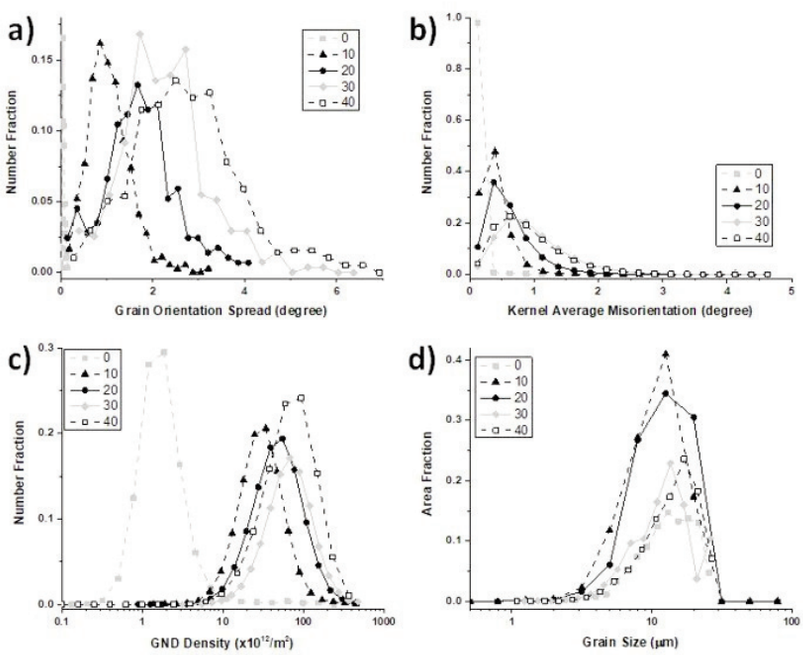

Figure 5. *a) Grain orientation spread (GOS, b) kernel average misorientation, c) geometrically necessary dislocation (GND) density and d) grain size distribution of the samples (legends indicate strain levels)*

Table 3. *EBSD and crystallographic texture analysis results*

Strain	EBSD data					Texture (MRD)			
(%)	KAM (degree)	GOS (degree)	Misorientation angle (degree)	GND density (x1012/m^2)	Grain Size (μm)	α fiber max intensity	α fiber average intensity	γ fiber max. intensity	γ fiber average intensity
0	0.0744	0.0741	35.6487	3.09446	14.1195	5.6537	1.973	20.7208	7.8452
10	0.3927	1.33	33.1589	39.8384	11.3184	5.3319	1.4237	24.0682	12.8366
20	0.6098	2.2116	25.1155	63.7319	13.0563	7.9239	2.6704	39.5356	10.096
30	0.9779	2.828	15.0229	91.0471	13.4267	15.6242	3.1059	29.4862	16.0676
40	0.9121	3.4999	12.1721	89.809	15.0333	19.2928	3.2728	30.2193	19.6909

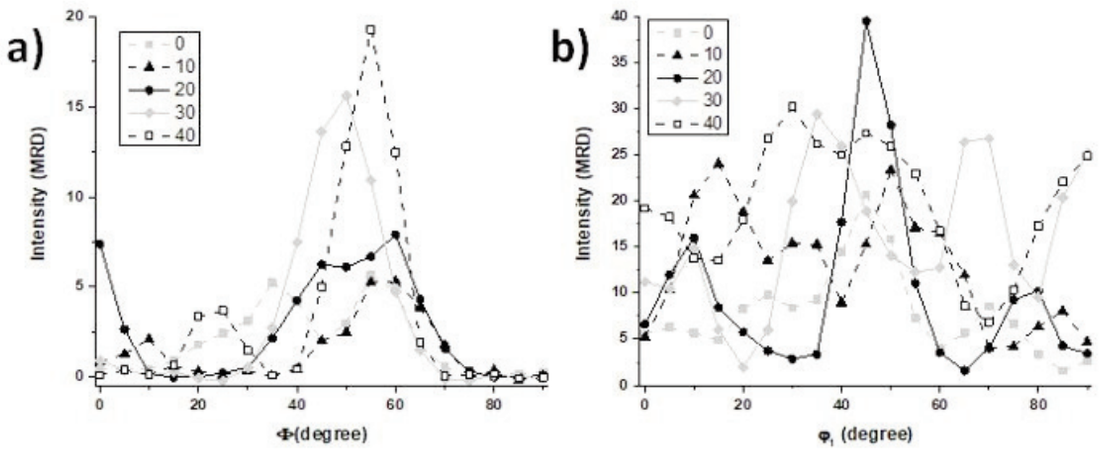

Figure 6. *Texture intensity distributions along a) α-fiber and b) γ-fiber*

4. Discussions

The results showed that the grain size, dislocation density, misorientations and crystallographic texture as well as hydrogen permeability values change with strain. To quantify the relation between these microstructural parameters and hydrogen diffusion, multiple linear regression analysis (MLRA) is used. MLRA should be performed by using independent input parameters that we know have a linear connection with the diffusion coefficient [40]. In this study, microstructural parameters are be used as input parameters to establish a model to predict the hydrogen diffusion coefficient. Independent input parameters were determined by checking the Pearson correlation coefficient (PCC). PCC determines whether a relationship exists between the variables, and if so, the direction and strength of this relationship. PCC is calculated when the two variables are numerical and at least one of them is distributed normally [41]. PCC ranges between -1 and 1. If PCC is equal to 1, this means there is perfect positive linear correlation and if PCC is equal to 0 this means there is no linear correlation. A negative PCC value indicates negative linear correlation.

The PCC values showing the correlations between microstructural parameters are given in Table 4. KAM, GOS, the misorientation angle and GND density values are intercorrelated (PCC > 0.94). As the deformation increases in the samples, the dislocation density and accordingly the grain orientation spread and misorienation values increase. Therefore, only GND was chosen as the input to the MLR model, since dislocations are potential trapping sites and their relationship with the diffusion constant is known. α-fiber intensity correlates well with GND density (PCC ~0.86). Because α-fiber increases with cold rolling ratio, the dislocation density also increases by the deformation.

Grain size and γ-fiber intensity values correlate very well (PCC between 0.81 - 0.94), as shown in Table 4. γ-fiber intensity increases with recrystallization, this mechanism also affects grain size. Fabian et al. found that ferrite grain size has no significant effect on hydrogen permeability in enamel steel in their study [25]. In other studies, the reduction of in grain size was found to have a positive effect on the hydrogen permeability property [16, 42]. Grain boundaries, dislocations, cavities, and microvoids have low binding energy and are reversible trapping sites. As the grain size decreases and dislocation density increases, the regions that act as barriers to prevent the movement of hydrogen atoms increase [16, 26, 42-45]. In this study grain boundaries are accepted as potential trapping sited. If grain boundaries are assumed to be spherical, then there should be a correlation between the grain surface area and the diffusion coefficient. For this reason, “grain size square” (GS-sqr) values are used in MLR.

Considering the dependence of microstructural parameters and previous studies, the square of grain size (GS-sqr) and GND density values were taken as independent input parameters and MLR analysis was performed. The results of MLRA including the regression coefficients between GS-sqr, GND density and diffusion coefficients are listed in Table 6. Moreover, the Analysis of Variance (ANOVA) table, which shows whether the regression models are significant or not, is given in Table 7. The df, SS, MS, F, p-value in the ANOVA tables define the degrees of freedom, the sum of squares, mean squares, continuous probability distribution and statistically significant difference, respectively. The model determined by MLRA is statistically significant ($p<0.05$). Experimentally determined hydrogen diffusion coefficients are compared to the ones predicted by MLRA in Figure 7. There is almost a perfect agreement between the MLRA and

Table 4. *PCC values showing correlations between microstructural parameters*

	KAM	GOS	Misorientation angle	GND density	Grain size	α fiber max. intensity	α fiber average intensity	γ fiber max. intensity	γ fiber average intensity
KAM	1								
GOS area	0.97	1							
Misorient angle	-0.96	-0.96	1						
GND number	0.99	0.97	-0.95	1					
Grain size area	-0.39	-0.26	0.32	-0.42	1				
Alpha fiber max.	0.89	0.9	-0.95	0.86	-0.19	1			
Alpha fiber average	0.86	0.81	-0.9	0.86	-0.56	0.84	1		
Gamma fiber max.	0.01	0.14	-0.02	-0.01	0.82	0.2	-0.29	1	
Gamma fiber average	-0.36	-0.23	0.36	-0.37	0.94	-0.26	-0.57	0.82	1

Table 5. *PCC values between strain, thickness, and H-diffusion*

	H- Diffusion Coefficient (cm^2/sec)	Mises Strain	Thickness	GND	GS-sqr
After Deformation (cm^2/sec)	1				
Mises Strain	-0.97	1			
Thickness	0.95	-0.99	1		
GND	-1	0.96	-0.93	1	
GS-sqr	-0.94	0.99	-1	0.93	1

experiments as the R^2 value is 0.99.

Sensitivity analysis was also performed using the linear model created by MLR analysis. Here, the effect of 10% increase or decrease in GND density or grain size on H-diffusion coefficient was investigated. The results of the sensitivity analysis are shown in Figure 8 as a tornado plot. The results show that the hydrogen diffusion coefficient is more sensitive to GND density. Forthe samplesstydied, the GND intensity varies between 3 and 90 (30-fold difference), and the square of grain size varies between 100 and 226 (2.26-fold difference). Because of this difference, the absolute value of the coefficient of GND is higher, which makes the diffusion constant more sensitive to GND. Moreover, interstitial atoms such as hydrogen dissolved in dislocations are more stable in this position as they reduce “overall lattice distortion”. Moving the hydrogen atoms away from this locally stable point in the matrix will create more lattice distortion. Because of this effect, dislocations are more effective trapping sites. This makes GNDs more effective on hydrogen diffusivity. Due to the open structure of the grain boundaries and their interconnectedness, grain boundaries have the effect of facilitating diffusion (also known as grain boundary diffusion mechanism). On the other hand, grain boundaries can act as trapping sites as well. For these reasons, the hydrogen diffusion coefficient is

Table 6. *Regression Coefficients obtained after MLRA*

	Coefficients	Standard Error	t Stat	P-value
Intercept	0.8785	0.0407	21.5934	0.0021
GND	-0.0043	0.0006	-7.7618	0.0162
GS-sqr	-0.0005	0.0004	-1.1643	0.3644

Table 7. *Anova table*

	df	SS	MS	F	Significance F
Regression	2	0.1332	0.0666	289.6641	0.0034
Residual	2	0.0005	0.0002		
Total	4	0.1337			

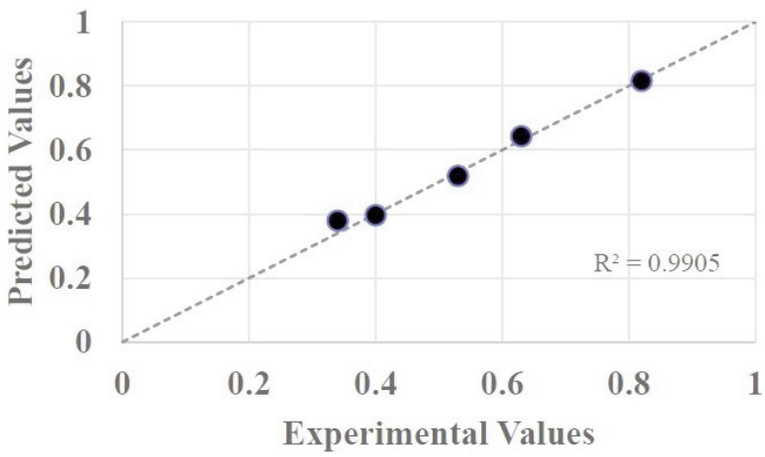

Figure 7. *Hydrogen diffusion coefficients obtained experimentally compared to ones predicted by MLRA*

more sensitive to GND density.

This new information can help to improve scaling resistance of enamel coatings and from a wider perspective hydrogen induced cracking and hydrogen storage properties of newly developed alloys.

5. Conclusions

Microstructural parameters such as grain size, crystallographic texture, dislocation density and misorientations as well as H-diffusion coefficient has been determined in a set of IF-steel samples that was deep drawn during Marciniak test until 40% strain

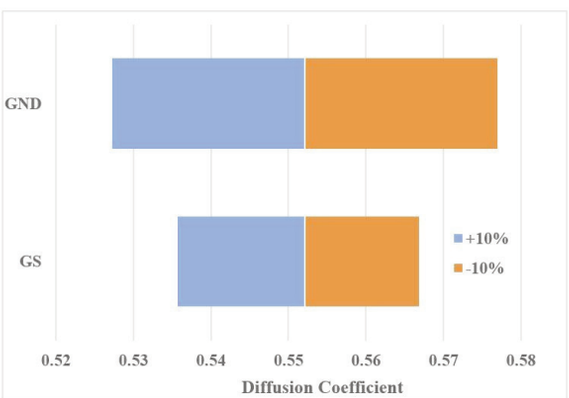

Figure 8. *Tornado plot showing the results of sensitivity analysis*

levels. The relation between hydrogen diffusion and microstructure was studied and quantified using multiple linear regression analysis. The following conclusions can be drawn:

Hydrogen diffusion coefficient decreases with increasing strain. Increasing strain increases misorientations, GND density, and changes grain structure as well as the intensity of crystallographic texture.

KAM, GOS, misorientation angle and GND density correlate well with each other since GND density calculation is based on local misorientations. Moreover, GND density correlates well with α-fiber intensity since this texture component intensifies with deformation. Grain size and γ-fiber intensity values also correlate well.

The results show a correlation between crystallographic texture and diffusion coefficient; however, this dependence is an indirect one since diffusion coefficient is isotropic in cubic materials. The differences in hydrogen diffusion coefficient are actually due to grain size and dislocation density differences.

Grain boundaries and dislocation cores act as trapping sites for hydrogen, therefore reducing its mobility. The sensitivity analysis shows that dislocations are more effective trapping sites than grain boundaries.

Grain boundaries not only act as trapping sites but also provide an additional mechanism easing diffusion (grain boundary diffusion). Therefore, they are less effective trapping sites than dislocation cores.

It should be noted that the correlations and coefficients presented here apply only to the present set of samples. Nevertheless, the results show which microstructural parameters H-diffusion coefficient is more sensitive to. Moreover, the methodology and parameters presented have general validity. This new information can be used to solve hydrogen-related problems in steels.

Authors contributions

U. Baskaya performed microstructural characterization and crystallographic texture analyses. R. Uzun carried out forming and hydrogen permeability tests. K. Davut made statistical analyses of EBSD data. U. Baskaya, R. Uzun, K. Davut and Y.

Kılıc evaluated the results of the tests and analyses. O. Gündüz assisted in the consideration of the manuscript.

Funding

The work has no any funding.

Conflict of interest

The authors declare that they have no known competing financial interests or personal relationships that could have appeared to influence the work reported in this paper.

References

[1] R.I.L. Guthrie, J.J. Jonas, in ASM Handbook, Volume 1, Properties and selection: irons, steels and high performance alloys, USA, 1993, p. 207-209, 666-667.

[2] S. Rossi, C. Zanella, R. Sommerhuber, Influence of mill additives on vitreous enamel properties, Materials and Design, (55) (2014) 880-887. https://doi.org/10.1016/j.matdes.2013.10.059

[3] K. Banerjee, Recrystallization, InTech, Rijeka, 2012, p. 153-163.

[4] M. Jitsukawa, Y. Hosoya, NKK's state-of-the-art flat-rolled products developed in the last decade, NKK Technical Review, 88 (2003) 46-57. https://doi.org/10.2298/JMMB170515033F

[5] https://constructalia.arcelormittal.com/files/A103_Enamelledsteel_brochure_EN_pdf2—60adb5707d099fd4af6f927e86b3181.pdf

[6] L. Falat, V. Homolova, L. Ciripova, A. Kroupa, The influence of isothermal ageing and subsequent hydrogen charging at room temperature on local mechanical properties and fracture characteristics of martensitic-bainitic weldments for power engineering, Journal of Mining and Metallurgy B: Metallurgy, 53 (3) (2017) 373-382. https://doi.org/10.2298/JMMB170515033F

[7] Y. S. Chen, P. A. Bagot, M. P. Moody, D. Haley, Observing hydrogen in steel using cryogenic atom probe tomography: A simplified approach, International Journal of Hydrogen Energy, 44(60) (2019) 32280-32291. https://doi.org/10.1016/j.ijhydene.2019.09.232

[8] Y. Sun, Y. F. Cheng, Hydrogen-induced degradation of high-strength steel pipeline welds: A critical review, Engineering Failure Analysis, 133 (2022) 105985. https://doi.org/10.1016/j.engfailanal.2021.105985

[9] X. Y. Cheng, H. X. Zhang, A new perspective on hydrogen diffusion and hydrogen embrittlement in low-alloy high strength steel, Corrosion Science, 174 (2020) 108800. https://doi.org/10.1016/j.corsci.2020.108800

[10] R. Valentini, S. Corsinovi, S. Barabesi, R. Zaccheroni, 23rd International Enamellers Congress, Florence, Italy, 2015, p. 13-22.

[11] W. Wan, Y. Y. Shan, K. Yang, Effect of TiN inclusions on the impact toughness of low-carbon microalloyed steels, Metallurgical and Materials Transactions A, 37 (7) (2006) 2147- 58. https://DOI:10.1007/BF02586135

[12] X. Huang, Z. Zhang, X. Liu, Y. Zhao, X. Li, Variations of microstructure and resistance to fish-scaling of a hot rolled enamel steel before and after enamel firing, Journal of Materials Research and Technology, 11 (2021) 466-473. https://doi.org/10.1016/j.jmrt.2021.01.048

[13] R. Valentini, A. Solina, L. Paganini, Model of hydrogen behaviour in enamelling grade steels, Part I Theory, Journal of Materials Science, 27 (1992) 6579-6582. https://doi.org/10.1007/BF01165939

[14] R. R. Danielson, W. H. Souder, Causes and control of fish scaling of enamels for sheet iron and steel, Journal of the American Ceramic Society, 4 (8) (2006) 620-654. https://doi.org/10.1111/j.1151-2916.1921.tb17363.x

[15] M. Leveaux, Z. Zermout, L. Moli Sanchez, I. Lizarraga Ferro, 24th International Enamellers Congress, Chigago, USA, 2018, p. 129-136.

[16] Z. Yi, W. Hongyan, D. Linxiu, 24th International Enamellers Congress, Chigago, USA, 2018, p. 115-122.

[17] X. Chun, Y. Ming, P. Linghuan, S. Quanshe, 24th International Enamellers Congress, Chigago, USA, 2018, p. 147-154.

[18] F. Dong, L. Du, X. Liu, F. Xue, Optimization of chemical compositions in low-carbon Al-killed enamel steel produced by ultra-fast continuous annealing, Materials Characterization, 84 (2013) 81-87. http://dx.doi.org/10.1016/j.matchar.2013.07.006

[19] E. R. Fábián, G. Csiszár, T. Ungár, Conference on Environmental Management and Engineering, Wuhan, China, 2011.

[20] A. J. Kumnick, H. H. Johnson, Deep trapping states for hydrogen in deformed iron, Acta Metallurgica, 28 (1979) 33-39. https://doi.org/10.1016/0001-6160(80)90038-3

[21] F. T. Dong, L. X. Du, X. H. Liu, J. Hu, F. Xue, Effect of Ti (CN) precipitation on texture evolution and fish-scale resistance of ultra-low carbon Ti-bearing enamel steel, Journal of Iron and Steel Research, International, 20(4) (2013) 39-45. https://doi:10.1016/S1006-706X(13)60080-1

[22] R. Uzun, Ü. Başkaya, Z. Çetin, Y. Kılıç, O. Gündüz, A. Bakkaloğlu, Effect of strain ratio on hydrogen permeability properties of low carbon enamel steel, Metallurgical Research and Technology, 118 (4) (2021) 412-420. https://doi.org/10.1051/metal/2021053

[23] M. A. Mohtadi-Bonab, M. Eskandari, J.A. Szpunar, Effect of arisen dislocation density and texture components during cold rolling and annealing treatments on hydrogen induced cracking susceptibility in pipeline steel, Journal of Materials Research, 31(21) (2016) 1-11. https://doi.org/10.1557/jmr.2016.357

[24] M. Barsanti, R. Ishak, R. Valentini, K. Sarrazy, S. Corsinovi, 24th International Enamellers Congress, Chigago, USA, 2018, p. 137-145.

[25] E.-R. Fábián, P. J. Szabó, Effect of texture on hydrogen permeability in low carbon Al-killed steels, Materials Science Forum, 659 (2010) 301-306. https://doi.org/10.4028/www.scientific.net/MSF.659.301

[26] E.-R. Fábián, Cold deformation effect on microstructure and on the hydrogen permeability of low carbon Al-killed steels, Materials Science Forum, 659 (2010) 7-12. https://doi:10.4028/www.scientific.net/MSF.659.7

[27] H. Takechi, Metallurgical aspects on interstitial free sheet steel from industrial viewpoints, Materials Science, 34 (1) (1994) 1-8. https://doi.org/10.2355/isijinternational.34.1

[28] https://www.gom.com/metrology-systems/aramis.html

[29] ASTM Standard G148-97 "Standard practice for evaluation of hydrogen uptake, permeation, and transport in metals by an electrochemical technique, ASTM International, West Conshohocken, PA, 2018.

[30] R. Valentini, M. De Sanctis, G. Lovicu, C. Colombo, 5th International Conference on Hydrogen Safety, Brussels, Belgium, 2013.

[31] ASTM Standard E2627-13, 2019, Standard practice for determining average grain size using electron backscatter diffraction (EBSD) in fully recrystallized polycrystalline materials, ASTM International, West Conshohocken, PA, 2019.

[32] P. Lejček, Grain Boundaries: Description, structure and thermodynamics, Grain Boundary Segregation in Metals, 136 (2010) 5-24. https://doi:10.1007/978-3-642-12505-8_2

[33] H. Mao, B. Li, Y. Du, A comprehensive analysis of three-dimensional normal grain growth of pure iron via multi-phase field simulation, Journal of Mining and Metallurgy, Section B: Metallurgy 57 (1) (2021) 105-114. https://doi:10.2298/JMMB191227007M

[34] J.F. Nye, Some geometrical relations in dislocated crystals, Acta Metallurgica 1 (2) (1953) 153-162. https://doi.org/10.1016/0001-6160(53)90054-6

[35] W. Pantleon, Resolving the geometrically necessary dislocation content by conventional electron backscattering diffraction, Scripta Materialia, 58 (11) (2008) 994-997. https://doi.org/10.1016/j.scriptamat.2008.01.050

[36] A. Arsenlis, D. M. Parks, Crystallographic aspects of geometrically-necessary and statistically-stored dislocation density, Acta Materialia, 47 (5) (1999) 1597-1611.https://doi.org/10.1016/S1359-6454(99)00020-8

[37] D. P. Field, P. B. Trivedi, S. I. Wright, M. Kumar, Analysis of local orientation gradients in deformed single crystals, Ultramicroscopy, 103 (1) (2005) 33-39. https://doi.org/10.1016/j.ultramic.2004.11.016

[38] R. Stanislav, O. Hilšer, V. Ochodek, L. Čížek, M. Kraus, V. Mareš, A. Grajcar, J. Švec, Effect of severe plastic deformation on mechanical and fatigue behavior of medium-C sheet steel, Journal of Mining and Metallurgy B: Metallurgy, 56 (2) (2020) 161-170. https://doi:10.2298/JMMB190910008R

[39] S. I. Wright, M. M. Nowell, D. P. Field, A review of strain analysis using electron backscatter diffraction, Microscopy and Microanalysis, 17 (3) (2011) 316-329. https://doi.org/10.1017/S1431927611000055

[40] G. K. Uyanık, N. Güler, A study on multiple linear regression analysis, Procedia - Social and Behavioral Sciences, 106 (2013) 234-240. https://doi.org/10.1016/j.sbspro.2013.12.027

[41] P. M. Sedgwick, Pearson's Correlation Coefficient, BMJ Clinical Research, 345 (2012) 1-2. https://doi.org/10.1136/bmj.e4483

[42] R. Valentini, A. Solina, S. Matera, Influence of titanium and carbon contents on the hydrogen trapping of microalloyed steels, Metallurgical and Materials Transactions A, 27 (1996) 3773-3780. https://doi.org/10.1007/BF02595626

[43] G. Gottstein, Physical foundations of materials science, 1st edition 2004.

[44] W. Y. Choo, J. Y. Lee, Thermal analysis of trapped hydrogen in pure iron, Metallurgical Transactions A, 13 (1982) 135-140. https://doi.org/10.1007/BF02642424

[45] W.Y. Choo, J.Y. Lee, Effect of cold working on the hydrogen trapping phenomena in pure iron, Metallurgical Transactions A, 14 (1983) 1299-1305. https://doi.org/10.1007/BF02664812

UTICAJ MIKROSTRUKTURE I KRISTALOGRAFSKE TEKSTURE NA DIFUZIJU VODONIKA U IF-ČELIKU

Ü. Başkaya [a*], R. Uzun [a], K. Davut [b], Y. Kiliç [a], O. Gündüz [a]

[a] Eregli železara i čeličana Co., R&D Centar, 67300, Kdz. Eregli, Zonguldak, Turska
[b] Odsek za nauku o materijalima i inženjerstvo, Institut za tehnologiju u Izmiru, Urla, Izmir, Turska

Apstrakt

Odnos između mikrostrukture, kristalografske teksture i difuzije vodonika proučavan je na IF čeliku. Uzorci čelika su duboko izvučeni do nivoa deformacije od 10%, 20%, 30% i 40%, a zatim su određivani koeficijenti difuzije vodonika korišćenjem Helios II sistema. Svetlosni mikroskop (LOM), skenirajući elektronski mikroskop (SEM) i difrakcija povratnog rasejanja elektrona (EBSD) korišćeni su za mikrostrukturnu karakterizaciju i studije kristalografske teksture. Zavisnost mikrostrukturnih parametara je procenjena korišćenjem vrednosti Pirsonovog koeficijenta korelacije (PCC). Ove procene su pokazale da su lokalne dezorijentacije, kristalografska tekstura i gustina dislokacija međusobno zavisne. PCC vrednosti pokazuju da su veličina zrna i gustina dislokacija nezavisni mikrostrukturni parametri. Ovi parametri su korišćeni za izgradnju modela za predviđanje koeficijenta difuzije vodonika metodom višestruke linearne regresione analize. Analiza osetljivosti je takođe izvršena sa ovim modelom da bi se razumelo na koji parametar je difuzija vodonika najosetljivija. Rezultati ove analize pokazuju da je difuzija vodonika osetljivija na gustinu dislokacija, što pokazuje da su dislokacije efikasnija mesta za hvatanje atoma vodonika. S druge strane, granice zrna su manje efikasna mesta za hvatanje jer takođe pružaju dodatni mehanizam difuzije.

Ključne reči: *Niskougljenični emajlirani čelik; Duboko izvlačenje; Permeabilnost vodonika; Mikrostruktura; Kristalografska tekstura; Analiza višestruke linearne regresije; Analiza osetljivosti*